Phase response of polarization-maintaining optical fiber to temperature changes

MARTIN KYSELAK[1*], FILIP DVORAK[2], JAN MASCHKE[1], CESTMIR VLCEK[1]

[1]Department of Electrical Engineering, Faculty of Military Technology,
 University of Defence, Kounicova 65, Brno, Czech Republic

[2]Department of Radar Technology, Faculty of Military Technology,
 University of Defence, Kounicova 65, Brno, Czech Republic

[*]Corresponding author: martin.kyselak@unob.cz

This paper deals with the phase shift development in the polarization-maintaining fiber owing to different temperatures of an applied defined body, where both polarization axes are excited. A variation of the Stokes parameters induced by the phase shift is expressed by the Jones matrix and a depiction on the observable Poincaré sphere. The temperature response of polarization-maintaining fiber and the effects of heat transfer on the phase shift variation of polarization-maintaining fiber were described theoretically. The time dependence of the phase shift development and its direction of rotation on the observable Poincaré sphere was measured and presented graphically. In addition, different response measures for higher and lower temperatures compared with the ambient temperature were experimentally evaluated.

Keywords: fiber sensor, polarization maintaining, optical fiber, observable Poincaré sphere, birefringence, temperature field disturbance.

1. Introduction

The proposed sensor of temperature field disturbance is based on the highly birefringent optical fiber, where both polarization axes are excited. By the effect of outer thermal energy and subsequent temperature change of the fiber, the velocity of propagating polarization modes is changed, with a subsequent phase shift between them.

The response of the fiber was evaluated for different configurations of the heat-exposed body and the fiber, different exposed lengths and fibers of different wavelengths. The results were regularly published [1–4].

For the construction of the sensor itself it is important to launch light output of defined polarization into the sensor fiber and also output light into a linear polarizer at a defined angle of polarization mode with respect to the polarization axes. In both cases it is necessary to provide insensibility of connecting parts of fibers to the outer effects, incidence of thermal energy in particular. Therefore, these parts of fiber were

provided with secondary protection. For a complete description of sensor behavior during laboratory evaluation, a polarimeter was used, making it possible to measure a complete set of parameters such as the Stokes parameters and the degree of polarization, and to derive from them useful data about the phase shift, propagation of optical waves under different conditions, *etc*.

For the needs of sensor property investigation, some measuring configurations of the above fiber system were proposed, namely for the connection of fibers by splices or by fiber connectors.

Earlier experiments have shown that the reaction of the sensor fiber to the effect of thermal source is quite complicated. Effects come to be exerted by emission, heat transport through air or by the circulation of air in the room. For these reasons, we tried to eliminate such effects and limited ourselves to only heat transfer by emission. This arrangement is described in detail in the experimental part.

For the measurement, we chose one from among the implemented configurations: input, sensor and output fibers, see Fig. 1. The slow axis of the input fiber is oriented in the *y*-axis of the chosen clockwise system of coordinates, and in this axis the linear polarized wave is excited. The sensor fiber is rotated such that the slow axis makes an angle of $\pi/4$ with the *y*-axis. In this case, the output fiber forms part of the sensor fiber covered with secondary protection. The output is oriented such that the slow axis is consistent with the *y*-axis of the coordinate system.

This paper focuses on the analytic description of the proposed arrangement by means of the Jones matrices and subsequently the Stokes parameters, which are measured and evaluated on the basis of polarimeter measurements. Additional data are obtained from experimental determination of the sensitivity and time responses of the system to the effect of defined body in the ambient temperature range. Similar measurements of the polarization state variation in highly birefringent fibers can also be found in [5–8].
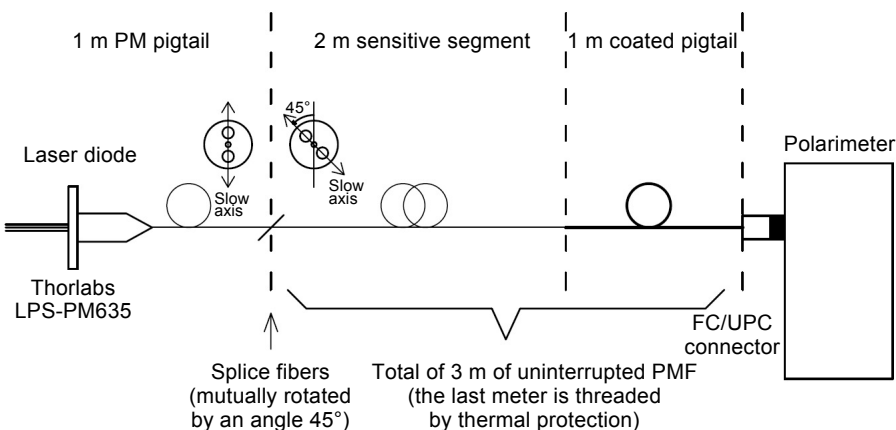

Fig. 1. Schematic arrangement for measurement of sensor fiber response.

2. Analytical description of sensor configuration

To achieve maximal sensor sensitivity, it is necessary to launch identically the two polarization modes of the fiber characterized by different refractive indexes. This condition can be fulfilled via circular polarization or by rotating the linear polarized light by π/4 with respect to the polarization axes. A disadvantage of the first possibility is the necessity of using a quarter-wave plate, which is difficult in the case of fiber configuration. Much better is the second method with identical excitation of both polarization planes provided by mutually rotating the source pigtail and the sensor fiber by an angle of π/4. This configuration can be implemented by means of oriented fiber fixation in the connector or by a splice with the same fiber orientation. Both variants are available in the laboratory but in the following text, only the splice variant prepared by SQS Company is studied. A schematic arrangement for the measurement of sensor fiber response is given in Fig. 1.

In the analytic description, we start from the ideal condition, where we do not consider inaccuracies in the set of mutual fiber angles, effect of torsion and bend with respect to the fiber configuration geometry, *etc*. The final coherence with respect to the bandwidth of the sources used is not considered either. The principle of sensor function is illustrated in Fig. 2.
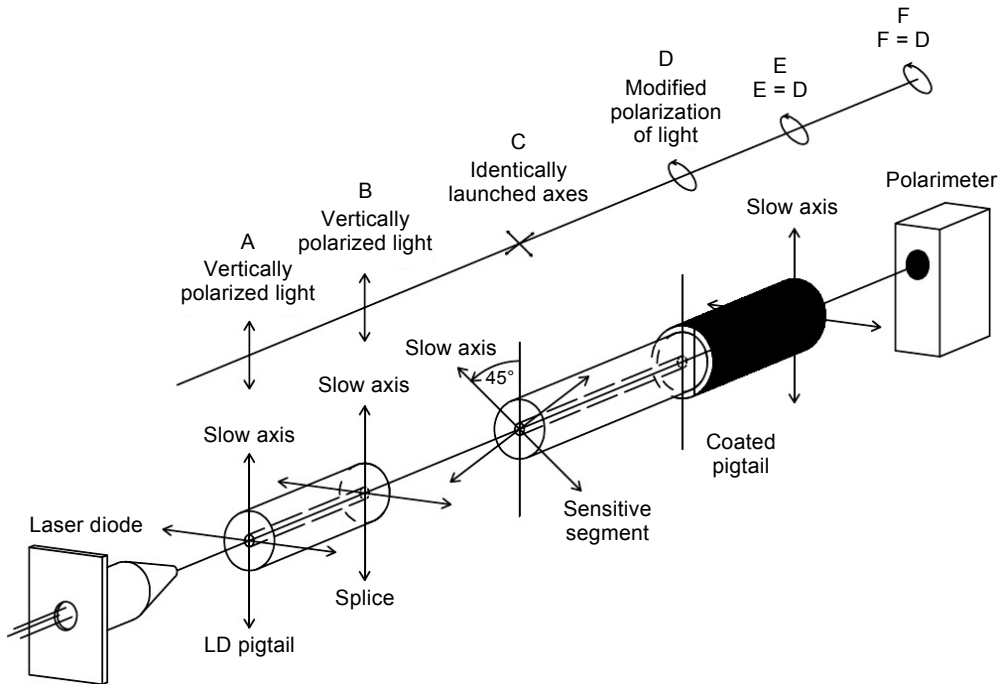

Fig. 2. Principle of sensor function.

The Jones matrix of a retarder rotated by a general angle ψ is

$$J_\psi = \begin{bmatrix} J_{xx} & J_{xy} \\ J_{yx} & J_{yy} \end{bmatrix} \tag{1}$$

where

$$J_{xx} = \cos^2(\psi)\exp(i\,\delta/2) + \sin^2(\psi)\exp(-i\,\delta/2)$$

$$J_{xy} = J_{yx} = \cos(\psi)\sin(\psi)\exp(i\,\delta/2) - \cos(\psi)\sin(\psi)\exp(-i\,\delta/2)$$

$$J_{yy} = \cos^2(\psi)\exp(-i\,\delta/2) + \sin^2(\psi)\exp(i\,\delta/2)$$

and δ is the phase shift between the slow and the fast polarization axes [9, 10].

By substituting $\psi = \pi/4$ in (1) we obtain

$$J_{\pi/4} = \begin{bmatrix} \cos(\delta/2) & i\sin(\delta/2) \\ i\sin(\delta/2) & \cos(\delta/2) \end{bmatrix} \tag{2}$$

The light with linear polarization in the *y*-axis excites the sensor fiber. We assume intensity, where the Jones vector at the sensor fiber input is given as $E[0 \;\; 1]^T$. If the output fiber orientation is identical with that in the input, that is to say there is no rotation in the connectors, the output electric field intensity described by the Jones vector will be

$$\begin{bmatrix} E_x \\ E_y \end{bmatrix} = \begin{bmatrix} \cos(\delta/2) & i\sin(\delta/2) \\ i\sin(\delta/2) & \cos(\delta/2) \end{bmatrix} E \begin{bmatrix} 0 \\ 1 \end{bmatrix} = E \begin{bmatrix} i\sin(\delta/2) \\ \cos(\delta/2) \end{bmatrix} \tag{3}$$

This equation is valid in the case when the slow axis is rotated by $\pi/4$ with respect to the *y*-axis. Because the slow axis is in the output identical with the *y*-axis, the output Jones vector must be transformed by rotating it by $-\pi/4$

$$\begin{bmatrix} E_{xr} \\ E_{yr} \end{bmatrix} = \frac{E}{\sqrt{2}} \begin{bmatrix} 1 & -1 \\ 1 & 1 \end{bmatrix} \begin{bmatrix} i\sin(\delta/2) \\ \cos(\delta/2) \end{bmatrix} = \frac{E}{\sqrt{2}} \begin{bmatrix} i\sin(\delta/2) - \cos(\delta/2) \\ i\sin(\delta/2) + \cos(\delta/2) \end{bmatrix}$$

$$= \frac{E}{\sqrt{2}} \begin{bmatrix} -\exp(-i\delta/2) \\ \exp(i\delta/2) \end{bmatrix} \tag{4}$$

In the fiber output, we obtained the corresponding Stokes parameters, measured in the experimental part: $S_0 = E^2$, $S_1 = 0$, $S_2 = -E^2\cos(\delta)$, and $S_3 = -E^2\sin(\delta)$.

The phase shift of a given polarization state on the observable Poincaré sphere (OPS) will be determined from the Stokes parameters [11]

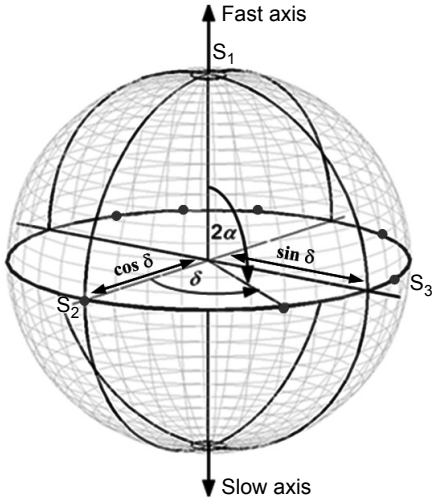$$\delta = \mathrm{atan}(S_3/S_2) \tag{5}$$

Fig. 3. Depiction of phase shift development on the observable Poincaré sphere (OPS).

The phase shift development can be depicted on the OPS [12] and it corresponds to a circle in the plane defined by the Stokes parameters S_2 and S_3 (see Fig. 3).

3. Polarization-maintaining fiber temperature response

For a phase shift δ with the reference ambient temperature v_0 it can be written

$$\delta_0(v_0) \; = \; \frac{2\pi}{\lambda}(n_c - n_{cl})l \; = \; \frac{2\pi}{\lambda}\Delta n_{eff}\, l \tag{6}$$

where λ is the wavelength, l is the exposed length of optical fiber, n_c and n_{cl} are the core and the cladding refractive indices, respectively, and Δn_{eff} is the differential refractive index.

For the temperature range considered, a linear dependence of the differential refractive index on the temperature can be assumed, *i.e.*,

$$\Delta n_{eff}(v) \; = \; \Delta n_{eff}(v_0) + \alpha\,\Delta v \tag{7}$$

where Δv is the temperature increase (°C), α is the temperature coefficient of Δn_{eff}. The temperature coefficient of Δn_{eff} can be written as

$$\alpha \; = \; \frac{\mathrm{d}\Delta n_{eff}}{\mathrm{d}v} \cong \frac{\Delta(\Delta n_{eff})}{\Delta v} \tag{8}$$

For the resulting phase shift, the following equation holds

$$\delta_\Sigma \; = \; \delta_0 + \delta \; = \; \frac{2\pi}{\lambda}l(\Delta n_{eff} + \alpha\,\Delta v) \tag{9}$$

The phase shift variation related to the ambient temperature phase shift is measured within the experimental work. The phase shift variation being measured can be written as follows:

$$\delta = \frac{2\pi}{\lambda} l \alpha \Delta \upsilon \tag{10}$$

If we know the values of the phase shift measured, the temperature variation and other parameters, the temperature coefficient of the Δn_{eff} could be determined [3, 13]. To determine this value, the condition of steady-state must be accomplished after the optical fiber has been exposed by the particular temperature of the body.

4. Heat transfer

The subject of examination is the heat transfer from an object with higher or lower temperature towards the optical fiber. In the initial state, the optical fiber temperature equals the ambient temperature. This also holds for the proposed arrangement of the sensor for the detection of temperature field disturbance. To be able to consider the optical fiber response dependence on the temperature field disturbance, the particular conditions need to be specified.

Let us assume that the temperature source is a body which is multiply heavier than the exposed optical fiber and its temperature does not vary within the experimental time. In a similar way, it is assumed that the ambient temperature does not vary either.

For the heat transfer evaluation, three transfer mechanisms are applied: conduction, convection and thermal radiation. The temperatures of individual components are described by indices: m for the excitation body, f for the optical fiber, and s for the surrounding area. The absolute temperature is described by the symbol T, the temperature in Celsius scale is denoted by the symbol υ.

Heat transfer by conduction depends on the thermal conductivity of the surroundings and on the temperature difference between the body and the optical fiber. Conduction is a function of temperature difference ($T_{\mathrm{m}} - T_{\mathrm{f}}$ or $\upsilon_{\mathrm{m}} - \upsilon_{\mathrm{f}}$). For convection, the function of temperature has a similar impact on heat transfer, but there are some differences. To define these heat transfer mechanisms is a difficult problem in view of the variation of optical fiber temperature and of the heat transfer conditions within the experimental time. To avoid these undefined conditions, an appropriate arrangement of the exposed optical fiber part was applied. By employing a plastic film cover, both undesired heat transfer mechanisms were suppressed. The arrangement applied resulted in a major impact of thermal radiation on heat transfer in this design of optical fiber sensor.

The rate at which energy is emitted, Q_{e} [W], is quantified by the Stefan–Boltzmann law [14]. The usual solutions to well-defined standard heat transfer problems cannot be applied in this case. Here the solution can be the application of a general consideration that the heat transferred between two bodies equals the difference of the fourth powers of their temperatures. For the heat transferred between a body and an optical

fiber Q_{mf} and the heat transferred between an optical fiber and the surroundings Q_{fs} it can be written

$$Q_{mf} = k_m(T_m^4 - T_f^4) \quad \text{and} \quad Q_{fs} = k_s(T_f^4 - T_s^4) \tag{11}$$

where k_m, k_s are the general heat transfer parameters depending on emissivity, area and shape of the body, general configuration, *etc*. and define radiation heat transfer.

For temperature equilibrium it holds

$$Q_{mf} - Q_{fs} = 0 \tag{12}$$

After substitution and modification, the relation for body temperature is obtained

$$T_m = X T_s \quad \text{and} \quad K_{ms} = \frac{k_m}{k_s} \tag{13}$$

where X is the ratio of the body temperature to the ambient temperature, K_{ms} is the ratio of general heat transfer parameters. For steady-state optical fiber temperature it can be written

$$T_f = T_s^4 \sqrt{\frac{X^4 K_{ms} + 1}{K_{ms} + 1}} \tag{14}$$

The relation defines the steady-state temperature of an optical fiber exposed to the excitation body whose temperature is different from the ambient temperature. The stabilized optical fiber temperature depends on the excitation body temperature, the ambient temperature and the ratio of general heat transfer parameters. Relation (14) is a qualitative expression, describing the tendency of temperature development from the viewpoint of both the sensitivity response and the dynamic response.

5. Arrangement of experimental workplace

The arrangement of the experimental workplace is shown in Fig. 4. The temperature source is represented by a plastic container with water. This layout allows selecting a higher or lower water temperature in comparison with ambient temperature, and it also allows adjusting different temperature steps. The water container is placed on polystyrene (PS) spacers and the PS cover of the measuring workplace. Inserted between the temperature source and the optical fiber sensor is a three-layer plastic wrap to suppress heat conduction and heat convection. To exclude any effect of outer disturbing sources and to prevent heat leakage, a polyethylene film is applied to the complete workplace as a delimiting cover. The water container exchanges heat with two lengths of optical fiber, which lie on a polystyrene board. From the three heat transfer mechanisms, thermal radiation is of the main impact in this configuration.

The light source was the laser diode LPS-PM635-FC (Thorlabs) mounted in a power supply controller LED driver DC2200 (Thorlabs). The optical power was launched into
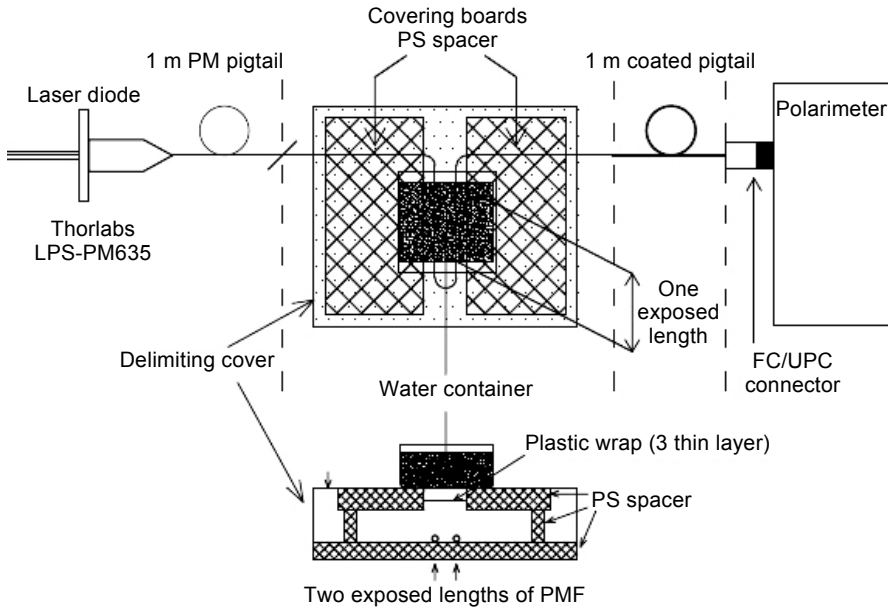
Fig. 4. Floor projection of measuring workplace with exposed length depiction and its sectional view.

the pigtail of the optical fiber PM630-HP Panda style. Linear vertical polarized (LVP) light was led into the sensor fiber via the splice. The angle of polarization axes was oriented 45° towards the LVP light (Fig. 2). The length of the optical fiber sensor part was 2 m and the sensor part was without secondary protection. The mutual angular rotation of polarization axes invoked almost the same excitation of both the slow axis and the fast axis of the optical fiber sensor part. The total length of exposed optical fiber sensor part was 54 cm. The output optical fiber was 1 m long and was coated with secondary protection to eliminate temperature effects and other outer disturbances. An FC/UPC connector terminated the optical fiber path and was inserted into the polarimeter PAN5710VIS Sensor Head (Thorlabs).

By applying the container with water, the excitation of exposed optical fiber length was invoked. The range of applied temperatures was from 0 to 48°C, the temperature step was 8°C and ambient temperature was 24°C. The temperature source was applied at the 140th second and removed at the 470th second. The total time of experimental measurement was 920 s and the laser diode operation current was 50 mA. The distance of the temperature source from the optical fiber sensor was defined by the PS spacer height and covering board thickness. Its value was 9 cm and the space between the covering boards was 12 cm.

6. Experimental results

The measurement was performed with the workplace arrangement according to Fig. 4. Experimental results were structured and divided into several parts. The fundamental

values were measured directly by a polarimeter, their further processing is subject to further research and discussion.

6.1. Values measured by polarimeter

We are concerned with periodic waveforms with a rising period corresponding to the process of radiation heating of the fiber. The measurement of the Stokes parameters is carried out continuously and attaching the container is performed after a period of 140 s, which is sufficient to capture the steady state before the excitation of the fiber. The settling time of the optical fiber response is relatively long due to ongoing measurement, and thus the heat source is not removed in a state of equilibration. For this reason, when evaluating the measurement, we are only concerned with baseline equilibration and attachment of the heat source.

Amplitude fluctuations are caused by the measurement method used, in particular the parameters of the polarimeter measuring head listed in the Table. The number of samples per unit time during the initial extreme change appears to be insufficient. The values of the Stokes parameters are normalized to the value 1 and their actual value is affected by phenomena such as coherence of optical waves of both polarizations, degree of polarization, *etc*.

T a b l e. Data values for measurement of polarization efficiency for polarization-maintaining fiber (PMF) 2 m of length, excited by LD635, exposure temperatures from 0 to +48°C with 8°C step (ambient temperature 24°C).

Optical source	LPS-PM635-FC
Basic sample rate	66.7 sps
Signal averaging	2
Result averaging	3
Sample time processing	0.18 s
Number of measurements	1024
Record rate	5
Sample time (record rate × sample time processing)	0.9 s

The measurements were done for exposure body temperatures of 0, 8, 16, 24, 32, 40, and 48°C. The following figures show examples of the waveforms of the parameters S_2 and S_3 at 0, 24 and 48°C. The exposure body was attached in the 139th to 140th second after the start of the measurement.

Waveforms of the S_2 and S_3 parameters for 0°C. A relatively precise temperature of 0°C was achieved using ice. Figure 5**a** shows the evolution of the parameter S_2, while Fig. 5**b** shows the evolution of the parameter S_3.

Evolution of the S_2 and S_3 parameters for 24°C (ambient temperature). The temperature 24°C was reached by letting water remain for a long time in the measured area, but still the water temperature differed from the measuring system temperature at the time of measurement, as is evidenced by the evaluation of the phase change in
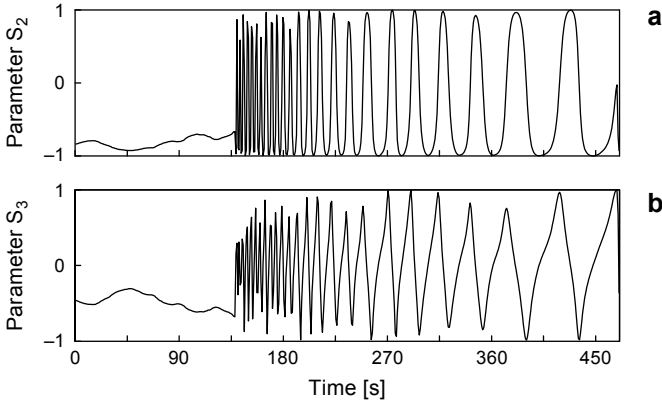
Fig. 5. Parameter S_2 (**a**) and S_3 (**b**) evolution for temperature excitation at 0°C.
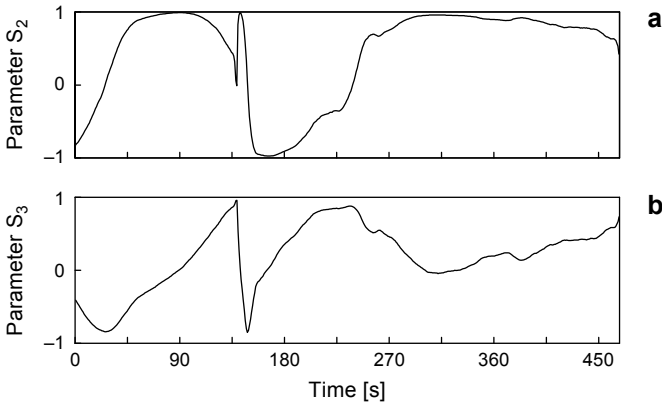

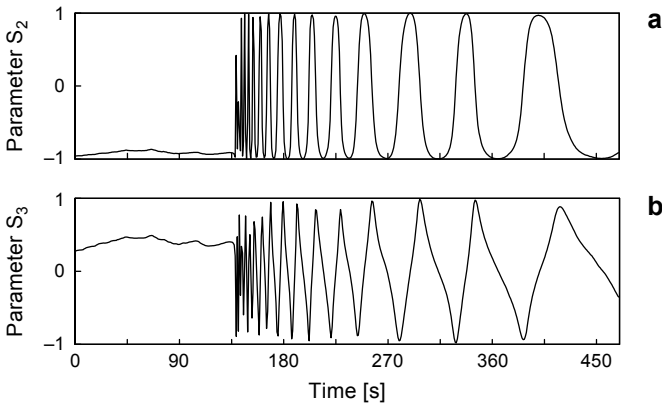Fig. 6. Parameter S_2 (**a**) and S_3 (**b**) evolution for temperature excitation at 24°C.

Fig. 7. Parameter S_2 (**a**) and S_3 (**b**) evolution for temperature excitation at 48°C.

Fig. 10. The deviation of the measured sample temperature from the system temperature is probably also a system error caused by the arrangement of the whole workplace and by the measuring method with minimal time of thermal stabilization of the system after a preceding measurement in the order of only minutes. Minor deviations are also caused by other factors such as the movement of people around the lab and the way the heat source is attached (by humans).

In Figs. 6, the S_2 and S_3 evolution parameters are shown for 24°C.

Evolution of the S_2 and S_3 parameters for 48°C. The presentation of results for a heat source having a temperature of 48°C was chosen for the purpose of clarity. The temperature is shifted mirror-wise to 0°C and to the mean ambient temperature of 24°C. Shown in Fig. 7 is the evolution of the parameters S_2 and S_3 for 48°C. When compared with the process at 0°C, it is obvious at a first sight that the optical fiber (OF) response to the excitation temperature is smaller.

6.2. Phase changes over time

An advantage of processing data measured by a polarimeter is the ease of processing the phase changes. The phase is thus determined with respect to the Stokes parameters and allows us to assess more clearly the consequences of heat effect. In Figure 8 the phase changes over time at 0, 24 and 48°C are presented. The graphs show the direction of the phase change when the body is attached.

The measured phase difference changes can be depicted on the OPS. It is thus possible to detect not only the change in operating temperature, but also to distinguish
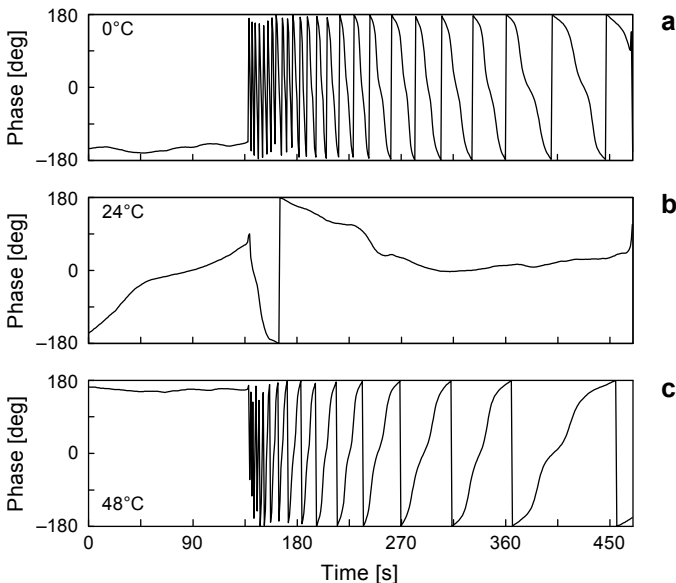

Fig. 8. The phase shift changes δ over time at 0°C (**a**), at 24°C (**b**), and at 48°C (**c**).

whether this temperature is higher or lower than the instantaneous temperature of the OF sensor.

For the negative phase shift $-\delta$, the phase curve slope during time is from the left to the right downwards (from 180° to −180°) and, conversely, for the positive phase shift $+\delta$, the phase curve slope during time is from the left to the right upwards (from −180° to 180°). When the heat source is removed, the steepness is inverted. It follows that for a negative phase shift, the direction of the development phase of polarization state is opposite to that of the positive phase shift.

From the measured experimental results as displayed on the observable Poincaré sphere, the direction is obvious of the evolution change for the negative phase shift in the clockwise direction while for the positive phase shift it is counterclockwise, as shown in Fig. 9.
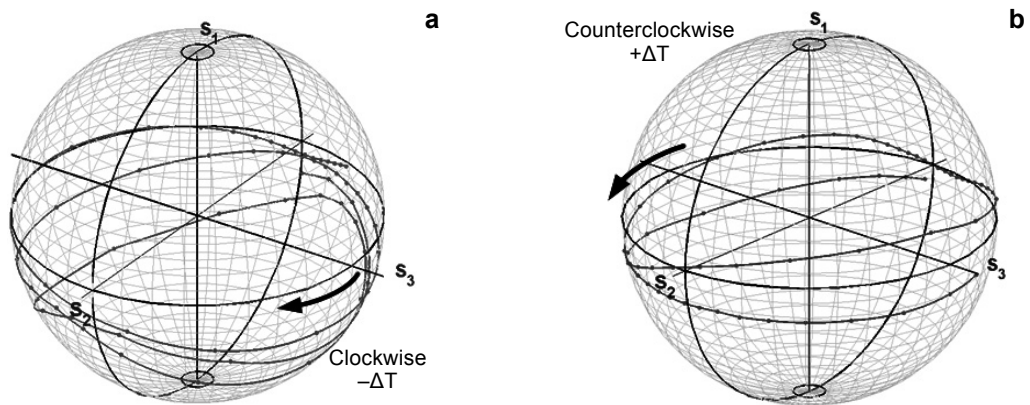

Fig. 9. The phase shift changes depicted on the OPS at applying heat source 16°C (clockwise) and 32°C (counterclockwise) in time interval from 161 to 215 s.

The phase shift development in Fig. 9 does not correspond to the ideal course of the evolution of the phase shift in Fig. 3. The reason for the different course of the phase shift development on an actual sensor consists in errors introduced by the OF splice, failing to reach the degree of polarization 1, fiber inhomogeneity, imperfect coherence, *etc.*

6.3. Phase shift changes over time for various temperatures

In Figure 10, the time-dependent phase shifts are shown for all exposure temperatures. From the waveforms, the difference is noticeable between exposure temperatures higher than the ambient temperature 24°C and lower temperatures.

This is due to different directions of the temperature gradient in these cases. While at higher temperatures the direction of the temperature gradient is from the exposure body, which is of larger mass, towards the fiber, at lower temperatures the direction is from the smaller-mass fiber of a higher temperature towards the larger-mass expo-
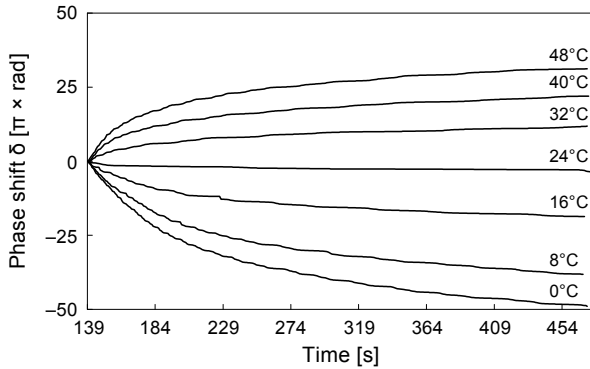
Fig. 10. The phase shift changes over time for temperatures from 0 to 48°C.

sure body of a lower temperature. Of significant importance is the fiber interaction with the surroundings, where the fiber continuously exchanges heat with the surroundings.

7. Discussion

Experimental results demonstrate the possibility of using a highly birefringent optical fiber as a sensor element. Shielding the sensor section from the effects of heat transfer by conduction and convection and highlighting the influence of heat transfer by radiation made it possible to achieve reproducible results.

During the experiments, the polarimeter was used for evaluating the polarization of the output optical radiation. Measuring the Stokes parameters and other parameters such as the degree of polarization, allows a deeper analysis of the problem than it would be in the case of a simple polarizer and a photodiode in the designed sensor. The main result is the fiber response to the temperature exposure of the body, expressed as the time dependence of phase shift changes. Some Stokes parameter waveforms, especially at the initial exposure time, can be influenced by the readings (for example the polarimeter sampling rate). It turns out, however, that this does not prevent the corresponding phase shift calculation.

The resulting waveform can also be affected by parasitic effects in the surroundings of the optical fiber. Due to the experimental configuration, it is possible to eliminate the influence of fiber torsion and bending on optical birefringence. With significant torque values and small bending radius, these fiber deformations may be influential.

The main result consists in the waveforms shown in Fig. 10, from which other partial dependence can be derived such as response to thermal exposure at certain times or dynamic properties. These issues will be addressed in the future work.

8. Conclusion

For defined conditions, the response of optical fiber to exposure invoked by an attached body of a particular temperature was investigated. The measurement reproducibility

was verified for these conditions and the main effect of thermal radiation was proved. The proposed optical fiber sensor configuration can be based on this heat transfer mechanism and on the suppression of undesirable heat transfer mechanisms like conduction and convection. In some applications, where the response of optical fiber to the thermal body excitation is studied, the effects of other heat transfer mechanisms can be included.

The aim of the work was to investigate the behavior of the proposed optical fiber sensor for defined conditions of suppressing outer disturbances, except for the defined heat effect. Out of the available sensor arrangements, the option with the well-defined conditions of optical light propagation was applied, namely the option with splice connections.

The reproducibility of measuring was verified for the defined conditions. Variations of proposed sensor arrangement can be extended from the sensor of thermal field disturbance to measuring the thermal radiation of bodies in the long-wave range or measuring the thermal radiation transmittance of plastic layers, *etc*.

Unlike measuring the optical intensity propagation on linear polarizer output, measuring the Stokes parameters allows analyzing the relations during optical light propagation, for example by investigating the state of polarization. This raises another question, concerning the relation between the state of polarization and the optical wave coherence depending on the spectral width of the source. Further research work will focus on examining the proposed sensor configuration from the viewpoint of light coherence and polarization degree. The application of angled physical contact instead of splice connection is also envisaged.

References

[1] KYSELÁK M., VLČEK Č., MASCHKE J., DVOŘÁK F., *Optical fibers with high birefringence as a sensor element*, Proceedings of 2016 IEEE 6th International Conference on Electronics Information and Emergency Communication (ICEIEC 2016), 2016, p. 190–193.

[2] DVORAK F., MASCHKE J., VLCEK C., *The response of polarization maintaining fibers upon temperature field disturbance*, Advances in Electrical and Electronic Engineering **12**(2), 2014, pp. 168–176.

[3] DVORAK F., MASCHKE J., VLCEK C., *The analysis of fiber sensor of temperature field disturbance by human body part access*, Advances in Electrical and Electronic Engineering **12**(6), 2014, pp. 575–581.

[4] DVOŘÁK F., MASCHKE J., VLČEK Č., *Utilization of birefringent fiber as sensor of temperature field disturbance*, Radioengineering **18**(4), 2009, pp. 639–643.

[5] FENG ZHANG, LIT J.W.Y., *Temperature and Strain Sensitivity Measurements of High-Birefringent Polarization-Maintaining Fibers*, Physics and Computer Science Faculty Publications, 1993.

[6] DOMANSKI A.W., *Polarization degree fading during propagation of partially coherent light through retarders*, Opto-Electronics Review **13**(2), 2005, pp. 171–176.

[7] LESIAK P., RAJAN G., SEMENOVA Y., FARRELL G., BOCZKOWSKA A., DOMAŃSKI A., WOLIŃSKI T., *A hybrid highly birefringent fiber optic sensing system for simultaneous strain and temperature measurement*, Photonics Letters of Poland **2**(3), 2010, pp. 140–142.

[8] SANG MIN JEON, YONG PYUNG KIM, *Temperature measurements using fiber optic polarization interferometer*, Optics and Laser Technology **36**(3), 2004, pp. 181–185.

[9] SHURCLIFF W., *Polarized Light, Production and Use*, Harvard University Press, Oxford University Press, Cambridge, London, 1962.

[10] BORN M.., WOLF E., *Principles of Optics*, 7th Ed., Cambridge University Press, 1999, pp. 556–570.

[11] COLLETT E., *Polarized Light in Fiber Optics*, Lincroft, New Jersey (USA), 2003.

[12] COLLETT B., SCHAEFER B., *Visualization and calculation of polarized light. I. The polarization ellipse, the Poincaré sphere and the hybrid polarization sphere*, Applied Optics **47**(22), 2008, pp. 4009–4016.

[13] CHIN-LIN CHEN, *Foundations for Guided-Wave Optics*, Wiley, New Jersey, 2007.

[14] MORAN M., SHAPIRO H., *Fundamentals of Engineering Thermodynamics*, 5th Ed., Wiley, USA, 2006.